A statics-dynamics equivalence through the fluctuation-dissipation ratio provides a window into the spin-glass phase from nonequilibrium measurements

M. Baity-Jesi,[1] E. Calore,[2] A. Cruz,[3, 4] L.A. Fernandez,[5, 4] J.M. Gil-Narvion,[4] A. Gordillo-Guerrero,[6, 4]
D. Iñiguez,[4, 7] A. Maiorano,[8, 4] E. Marinari,[8, 9] V. Martin-Mayor,[5, 4] J. Monforte-Garcia,[4]
A. Muñoz-Sudupe,[5, 4] D. Navarro,[10] G. Parisi,[8, 9] S. Perez-Gaviro,[11, 4] F. Ricci-Tersenghi,[8, 9]
J.J. Ruiz-Lorenzo,[12, 4] S.F. Schifano,[13] B. Seoane,[14, 4] A. Tarancon,[3, 4] R. Tripiccione,[2] and D. Yllanes[15, 4]

(Janus Collaboration)

[1]*Institut de Physique Théorique, DRF, CEA Saclay, F-91191 Gif-sur-Yvette Cedex, France*
[2]*Dipartimento di Fisica e Scienze della Terra, Università di Ferrara e INFN, Sezione di Ferrara, Ferrara, Italy*
[3]*Departamento de Física Teórica, Universidad de Zaragoza, 50009 Zaragoza, Spain*
[4]*Instituto de Biocomputación y Física de Sistemas Complejos (BIFI), 50009 Zaragoza, Spain*
[5]*Departamento de Física Teórica I, Universidad Complutense, 28040 Madrid, Spain*
[6]*Departamento de Ingeniería Eléctrica, Electrónica y Automática, U. de Extremadura, 10071, Cáceres, Spain*
[7]*Fundación ARAID, Diputación General de Aragón, Zaragoza, Spain*
[8]*Dipartimento di Fisica, Sapienza Università di Roma,*
Istituto Nazionale di Fisica Nucleare, Sezione di Roma I, I-00185 Rome, Italy
[9]*Nanotec-Consiglio Nazionale delle Ricerche, I-00185 Rome, Italy*
[10]*Departamento de Ingeniería, Electrónica y Comunicaciones and I3A, U. de Zaragoza, 50018 Zaragoza, Spain*
[11]*Centro Universitario de la Defensa, Carretera de Huesca s/n, 50090 Zaragoza, Spain*
[12]*Departamento de Física and Instituto de Computación Científica Avanzada (ICCAEx),*
Universidad de Extremadura, 06071 Badajoz, Spain
[13]*Dipartimento di Matematica e Informatica, Università di Ferrara e INFN, Sezione di Ferrara, Ferrara, Italy*
[14]*Laboratoire de Physique Théorique, École Normale Supérieure & Université de Recherche Paris Sciences et Lettres,*
Pierre et Marie Curie & Sorbonne Universités, UMR 8549 CNRS, 75005 Paris, France
[15]*Department of Physics and Soft Matter Program, Syracuse University, Syracuse, NY, 13244*
(Dated: April 7, 2017)

The unifying feature of glass formers (such as polymers, supercooled liquids, colloids, granulars, spin glasses, superconductors, ...) is a sluggish dynamics at low temperatures. Indeed, their dynamics is so slow that thermal equilibrium is never reached in macroscopic samples: in analogy with living beings, glasses are said to age. Here, we show how to relate experimentally relevant quantities with the experimentally unreachable low-temperature equilibrium phase. We have performed a very accurate computation of the non-equilibrium fluctuation-dissipation ratio for the three-dimensional Edwards-Anderson Ising spin glass, by means of large-scale simulations on the special-purpose computers Janus and Janus II. This ratio (computed for finite times on very large, effectively infinite, systems) is compared with the equilibrium probability distribution of the spin overlap for finite sizes. The resulting quantitative statics-dynamics dictionary, based on observables that can be measured with current experimental methods, could allow the experimental exploration of important features of the spin-glass phase without uncontrollable extrapolations to infinite times or system sizes.

Theory and Experiment follow apparently diverging paths when studying the glass transition. On the one hand, experimental glass formers (spin glasses, fragile molecular glasses, polymers, colloids, ...) undergo a dramatic increase of characteristic times when cooled down to their glass temperature, T_g [1]. Below T_g, the glass is always out of equilibrium and *aging* appears [2]. Consider a rapid quench from a high temperature to the working temperature T ($T < T_g$), where the system is left to equilibrate for time t_w and probed at a later time $t + t_w$. Response functions such as the magnetic susceptibility turn out to depend on t/t_w^μ, with $\mu \approx 1$ [2–4]. The age of the glass, t_w, remains the relevant time scale even for t_w as large as several days. Relating the aging experimental responses to equilibrium properties is an open problem.

A promising way to fill the gap is to establish a statics-dynamics dictionary (SDD) [5–8]: non-equilibrium properties at *finite times* t, t_w, as obtained on samples of macroscopic size $L \to \infty$, are quantitatively matched to

equilibrium quantities computed on systems of *finite size* L [the SDD is an $L \leftrightarrow (t, t_w)$ correspondence]. Clearly, in order for it to be of any value, an SDD cannot strongly depend on the particular pair of aging and equilibrium quantities that are matched.

Some time ago, we proposed one such a SDD [6–8]. However, this SDD was unsatisfactory in two respects. First, L was matched only to t_w (irrespectively of the probing time $t + t_w$). Second, our SDD matched spatial correlation functions whose experimental study is only incipient [9, 10].

One could think [5] of building an SDD through the Generalized Fluctuation Dissipation relations (GFDR) first introduced in [11] (for related developments see [12–19]). The GFDR are correct at very large times. However, on time scales that can be investigated in experiments, glassy systems are not fully thermalized since the approach to equilibrium is very slow. Strong corrections pollute GFDR at finite times. Here we show how the

SDD can be used in a particular case to compute such corrections (that will be likely present in all glassy systems). We find that the naive implementation of this idea [5] does not work in general, and we introduce a modified SDD that works for spin glasses (and, hopefully, also for glasses).

GFDR carry crucial information [11, 14, 15]: they provide a promising experimental path towards measuring Parisi's functional order parameter [20]. As a consequence GFDR have attracted much attention. One encounters numerical studies for both Ising [13, 16, 18] and Heisenberg [21, 22] spin glasses, as well as for structural glasses [23–27]. On the experimental side, we have studies on atomic spin glasses [17, 19], superspin glasses [10], polymers [9, 28], colloids [29–35] or DNA [36].

Here, we perform a detailed simulation of GFDR in the three-dimensional Ising spin glass employing the custom-made supercomputers Janus [37] and Janus II [38]. In fact, this has been the launching simulation campaign of the Janus II machine, which was designed with this sort of dynamical studies in mind. Our simulations stand out by the spanned time range (11 orders of magnitude), by our high statistical accuracy and by the range of system sizes, enabling us to control size effects ($L = 20$, 40, 80 and 160). Thus armed, we assess whether or not an SDD can be built from the GFDR, and compare the SDD proposed in this paper with other proposals. We focus on spin glasses, rather than on other model glasses, for a number of reasons: (i) their sluggish dynamics is known to be due to a thermodynamic phase transition at $T_c = T_g$ [39–41]; (ii) the linear size of the magnetically correlated domains, $\xi(t_w)$, is experimentally accessible [42, 43] ($\xi \sim 100$ lattice spacings [42], much larger than comparable measurements for structural glasses [44]); (iii) a GFDR-based SDD has been well established in the limit of large sizes and times [11, 14, 15], see (4) below; (iv) GFDR have been studied experimentally [17]; (v) well developed, yet mutually contrasting, theoretical scenarios are available for spin glasses in equilibrium [45]; (vi) magnetic systems are notably easier to model and to simulate numerically (in fact, special-purpose computers have been built for the simulation of spin glasses [37, 38, 46–48]).

GFDR and the SDD We suddenly cool a three-dimensional spin-glass sample of size L^3 from high temperature to the working (sub-critical) temperature $T = 0.7 = 0.64T_c$ at the initial time $t_w = 0$ (see Methods, below, for more details and definitions). During the non-equilibrium relaxation a coherence length $\xi(t_w)$ grows [6, 42, 49], which is representative of the size of the spin-glass domains. Then, from the waiting time t_w on, we place the system under a magnetic field of strength H, and consider the response function at a later measuring time $t + t_w$

$$\chi_L(t + t_w, t_w) = \left.\frac{\partial m_L(t + t_w)}{\partial H}\right|_{H=0}, \qquad (1)$$

where $m_L(t+t_w)$ is the magnetization density in a sample of linear size L. This susceptibility is then compared with the spin temporal correlation function $C_L(t+t_w, t_w)$. From now on, we shall take the limits

$$\chi(t + t_w, t_w) = \lim_{L\to\infty} \chi_L(t + t_w, t_w), \qquad (2)$$

$$C(t + t_w, t_w) = \lim_{L\to\infty} C_L(t + t_w, t_w), \qquad (3)$$

which are easy to control numerically: if $L \gtrsim 7\xi(t + t_w)$ size effects are negligible [6][50] (see also Appendix F).

The Fluctuation Dissipation Theorem (FDT) states that $T\chi(t + t_w, t_w) = 1 - C(t + t_w, t_w)$, with both χ and C computed at $H = 0$. However, for $T < T_c$ the FDT does not hold. In fact, GFDR take the form [11, 14, 15] (the order of limits is crucial):

$$\lim_{t_w\to\infty} T\chi(t + t_w, t_w) = \lim_{t_w\to\infty}\left[\lim_{L\to\infty} S(C_L(t + t_w, t_w), L)\right], \qquad (4)$$

where t is scaled as t_w grows, to ensure that the full range $0 < C(t + t_w, t_w) < 1$ gets covered, and $S(C, L)$ is given by a double integral of $P(q, L)$, the equilibrium distribution function of the spin overlap, whose explicit definition is provided in the Methods Section.

Here, we mimic an experimental protocol [17, 19] in that we consider the non-equilibrium response on a very large system but at *finite times*. We try to relate this response with the equilibrium overlap for a system of finite effective size L_{eff}

$$T\chi(t + t_w, t_w) = S\big(C(t + t_w, t_w), L_{eff}(t + t_w, t_w)\big), \qquad (5)$$

where we have assumed that both χ and C have reached their thermodynamic limit. The same approach was followed for a two-dimensional spin glass by Barrat and Berthier [5] (note, however, that there is no stable spin-glass phase at $T > 0$ in two spatial dimensions).

Eq. (5) provides a statics-dynamics dictionary (SDD) relating both times t and t_w with a single effective equilibrium size $L_{eff}(t + t_w, t_w)$. Note that it is not obvious a priori that our program can be carried out. For instance, our SDD does not exist for ferromagnets, as explained in details in Appendix H exploiting data from Refs. [51, 52].

SDDs based on the comparison of aging and equilibrium correlation functions (rather than on GFDR) have been studied in some detail [7, 8, 53]. It was found that the effective length depends solely on t_w. Indeed,

$$L_{eff}(t + t_w, t_w) = k\,\xi(t_w), \qquad (6)$$

with $k \approx 3.7$, was accurate enough to match the correlation functions [7, 8]. Ref. [5] also agreed with (6). In fact, (6) also underlies the analysis of Refs. [54, 55]. Yet, we shall show below that (6) is oversimplified.

Numerical data The three basic quantities computed in this work, namely $\chi(t+t_w, t_w), C(t+t_w, t_w)$ and $\xi(t_w)$ are displayed in Fig. 1. Full details about this computation are provided in Appendix C.

Let us remark that the Janus II supercomputer allows us to probe unexplored dynamical regimes, either t/t_w
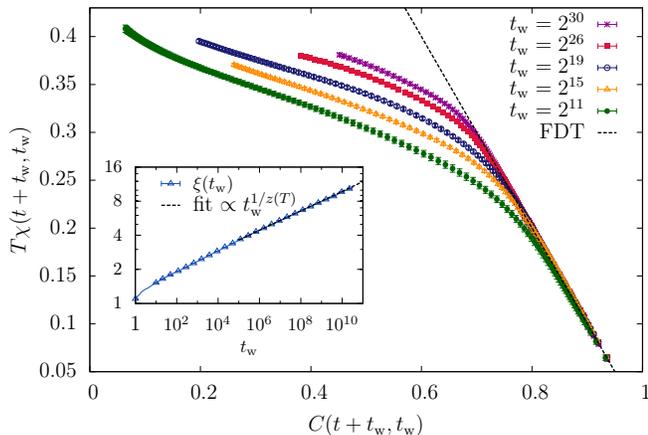
FIG. 1. Response function $T\chi(t+t_w, t_w)$ versus $C(t+t_w, t_w)$ at $T = 0.7$ [for fixed t_w, $C(t+t_w, t_w)$ monotonically decreases from $C = 1$ at $t = 0$ to $C = 0$ at $t = \infty$]. Data for $t_w = 2^{11}$ and $t_w = 2^{30}$ were obtained on Janus II (the other t_w are from Janus). The five values of t_w correspond to effective equilibrium sizes L_{eff} that, according to (6), span the size range investigated in Ref. [7] (namely, $8 \leq L \leq 32$). **Inset:** growth of the spin-glass coherence length $\xi(t_w)$ as a function of time, computed at zero magnetic field and following Refs. [6, 49], from simulations of $L = 160$ lattices at $T = 0.7$ on Janus II. In dashed lines we plot the scaling $\xi(t_w) \propto t_w^{1/z(T)}$ with $z(T) = 11.64$ from Ref. [48].

FIG. 2. Close-up of Fig. 1 (we only show data for three t_w, for the sake of clarity). Lines are $S(C, L_{\text{eff}})$, recall (5), with the effective equilibrium size as in (6): $L_{\text{eff}}(t + t_w, t_w) = k\xi(t_w)$. Dotted lines correspond to $k = 3.7$, which is the proportionality constant that was found by matching equilibrium and non-equilibrium correlation functions [6–8]. The continuous lines were found by choosing the best possible k for each t_w. This representation shows that the single-time statics-dynamics dictionary $L_{\text{eff}} \sim \xi(t_w)$ breaks down for large t, when $\xi(t + t_w)$ is much larger than $\xi(t_w)$.

as large as $2^{24} \approx 1.4 \times 10^7$ (i.e., we follow the magnetic response for a very long time, after the field was switched on at $t_w = 2^{11}$) or t_w as large as 2^{30} (i.e., we study the response of a very old spin glass, but we are limited to $t/t_w \approx 27$ in this case).

It is also remarkable that we are able to compute both the susceptibility χ and the correlation function C without worrying about finite-size effects. Indeed, size effects become visible when the coherence length reaches the threshold $\xi(t_w) \approx L/7$ [6] which in our $L = 160$ lattice translates to $\xi \approx 23$ lattice spacings. As Fig. 1–inset shows, we are quite far from this safety threshold.

With respect to previous measurements of the GFDR ratio, it is worth stressing that now we are able to take the $h \to 0$ limit in a more controlled way. This is far from trivial, given that the linear response regime shrinks to very small field when t_w increases (see Appendix C).

The data in Fig. 1 also stand out by their statistical accuracy (due to the large number of samples and large system sizes we simulated, but also thanks to the analysis method described in Appendix D As a consequence, a behavior different from the one implied by FDT, $T\chi(t, t_w) = 1 - C(t, t_w)$ can be studied in detail. In particular, the reader might be stricken by the linear behavior at $C(t + t_w, t_w) \approx 0.4$. In fact, following Refs. [11, 14, 15], this linear behavior could be interpreted as evidence for one step of replica-symmetry breaking (see, for instance, Ref. [56]). However, we shall argue below that the effective length in (5) evolves as
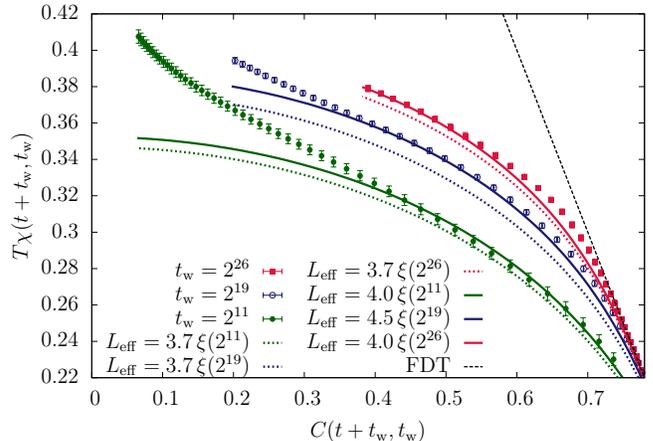
time t grows, thus producing an upturn in the response which is probably responsible for the linear behavior in Fig. 1.

Let us make a final remark. We know that $S(C, L)$ is upper bounded by $1 - \overline{\langle |q| \rangle}_{L=\infty} \geq 1 - q_{\text{EA}}^{(L=\infty)}$ (see Methods for definitions; the proof of the inequality is outlined in Appendix G). At $T = 0.7$ we know that $1 - q_{\text{EA}}^{(L=\infty)} = 0.48(3)$ [8] (or $0.46(3)$ [7]). Therefore, the dynamic responses $T\chi(t, t_w)$ in Fig. 1 are well below $1 - q_{\text{EA}}^{(L=\infty)}$ and (5) could be satisfied. The general conditions under which (5) can be used are discussed in the Appendix.

The effective equilibrium size As we show in Fig. 2, our data are too accurate to be quantitatively described by combining (5) with (6). This simple description fails both at short times t (i.e., when $C(t, t_w) \approx q_{\text{EA}}^{[L \approx 4\xi(t_w)]}$) and also at very long t, although one can find a constant k that works well for intermediate t.

The discrepancy for long t seems easy to rationalize: since the growth of $\xi(t_w)$ is very slow, recall Fig. 1–inset, $\xi(t + t_w)$ and $\xi(t_w)$ are very similar to each other for small t and, therefore, $L_{\text{eff}} \propto \xi(t_w)$ makes sense. However, since $\xi(t_w)$ grows without bounds in the spin-glass phase, one should eventually have $\xi(t + t_w) \gg \xi(t_w)$. Under these circumstances, it is only natural that $L_{\text{eff}} \propto \xi(t + t_w)$.

We can test this proposal by computing an exact L_{eff} for each (t, t_w) pair (see Appendix E for details), which we plot in Fig. 3: in the main panel in units of $\xi(t + t_w)$ and in the inset in units of $\xi(t_w)$.
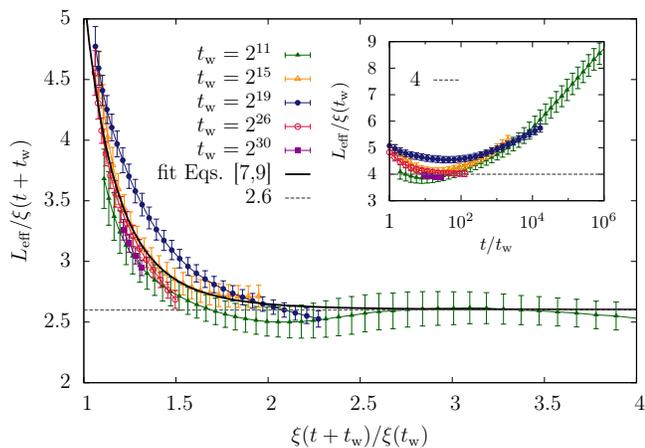
FIG. 3. For each t_w, we show the effective equilibrium size $L_{eff}(t+t_w, t_w)$ in units of the coherence length at the measuring time $\xi(t + t_w)$ versus the ratio of coherence lengths $\xi(t + t_w)/\xi(t_w)$ (recall that t is the time elapsed since switching-on the magnetic field). The ratio of coherence lengths is 1 for $t = 0$ and goes as $\xi(t + t_w)/\xi(t_w) \propto (1 + t/t_w)^{1/z(T)}$ for large time, with $z(T = 0.7) = 11.64(15)$ [49]. Let us stress that there is no extrapolation in this figure, only interpolation (i.e., L_{eff} falls within the simulated equilibrium sizes, $8 \leq L_{eff} \leq 32$). The solid line is a fit to the scaling function $h(x)$ in (7) and (9). **Inset:** $L_{eff}(t+t_w, t_w)$ data from the main panel in units of the coherence length at the initial time time $\xi(t_w)$, as a function of the time ratio t/t_w.

The first important observation from the main panel in Fig. 3 is that, for long enough times, we find $L_{eff} \approx 2.6\,\xi(t + t_w)$, in agreement with the intuition exposed above. This is definitely different from (6), used until now. The data in the inset of Fig. 3 explain why the previous relation in (6) passed many numerical tests until now: the non-monotonic behavior of $L_{eff}/\xi(t_w)$ for short times t makes this ratio roughly compatible with a constant $k \approx 4$ as long as $t/t_w \lesssim 1000$.

Surprisingly, the ratio $L_{eff}/\xi(t + t_w)$, or equivalently $L_{eff}/\xi(t_w)$, becomes large as well when $t \to 0$, thus explaining the inability of (5) in describing dynamical data at short times t (see Fig. 2). Nonetheless in the limit $t \to 0$, i.e. $\xi(t + t_w)/\xi(t_w) \to 1$, the effective equilibrium size L_{eff} seems to reach a finite value; a divergence of L_{eff} in this limit seems unlikely (see Appendix I).

L_{eff} *and the spin-glass coherence length* Now that it is clear that both $\xi(t_w)$ and $\xi(t + t_w)$ are relevant for L_{eff} one may ask about the crossover between the $\xi(t_w)$-dominated regime and the $\xi(t + t_w)$-dominated regime. Fig. 3 tells us that $L_{eff}/\xi(t+t_w)$ is, to a good approximation, a function of the ratio $\xi(t+t_w)/\xi(t_w)$.[57] Thus, we attempted to fit the crossover with the functional form

$$L_{eff}(t + t_w, t_w) = \xi(t + t_w)\, h\big(\xi(t + t_w)/\xi(t_w)\big)\,, \quad (7)$$

where the scaling function is

$$h(x) = k_1 \; + \; k_2\, x^{-c}\,. \quad (8)$$

Interpolation of data shown in Fig. 3 returns: $k_1 = 2.58(2)$, $k_2 = 2.7(1)$ and $c = 5.9(2)$. Noticing that $k_2 \approx k_1$ and $c \approx z(T)/2$, where $z(T)$ is the exponent for the time growth of the coherence length, $z(T = 0.7) = 11.64(15)$ (see Fig. 1–inset, and Refs. [6, 49]), the scaling function $h(x)$ can be also rewritten in a much simpler form as

$$h\big(\xi(t + t_w)/\xi(t_w)\big) = k_1 \left(1 + \sqrt{\frac{t_w}{t + t_w}}\right) \quad (9)$$

Fitting data in Fig. 3 with this simpler scaling function returns $k_1 = 2.59(1)$ (see full curve in Fig. 3). Given that the fit with 3 adjustable parameters in (8) and the one in (9) with just 1 adjustable parameter have practically the same quality-of-fit, we tend to prefer the simpler ansatz, as long as it interpolates the numerical data well enough.

The ultimate check for the success of (7) and (9) in reproducing the aging response is provided by Fig. 4, where the dynamical measurements (data points with errors) are plotted together with the equilibrium function $S(C(t + t_w, t_w), L_{eff}(t + t_w, t_w))$. The very good agreement in the whole range gives a strong support in favor of an SDD based on (7) and (9).

Note as well that (7) explains the previous success of the simpler SDD in (6). In fact, at short times t, the two coherence lengths $\xi(t + t_w)$ and $\xi(t_w)$ are very similar to each other, and the amplitude k in (6) is essentially $k = k_1 + k_2 \approx 2k_1$.

The ansatz of (7) provides as well a simple explanation for the upturn of the aging response at small values of C, recall Fig. 1. Indeed, as time t increases, the correlation function decays as $C \propto (t + t_w)^{-1/\alpha}, \alpha \approx 7$ [6]. But, from $\xi(t + t_w) \propto (t + t_w)^{1/z(T)}$ we conclude that, even at fixed t_w, L_{eff} diverges for large t as $C^{-\alpha/z(T)}$. Now, to a first approximation, one may expect that $S(C, L = \infty) - S(C, L) \propto L^{-\theta \approx -0.38}$ (see the description of the overlap distribution function in the Methods section, below). We thus expect the susceptibility to approach its $C = 0$ limit in a singular way, as $C^{\theta/(\alpha z(T))} \approx C^{0.23}$.

Which features of the $P(q)$ can be obtained from dynamic measurements? One of the major gains of the present analysis would be to obtain Parisi's functional order parameter $P(q)$ from experimental dynamic data. In an ideal situation, one would have data for χ, C and ξ, complemented by the ansatz in (9). Then, one would like to know which features of the underlying $S(C, L)$ can be retrieved from these dynamic measurements.

In order to answer this question, we have considered a very simplified $P_{simpl}(q, L)$, that possesses the main features of the $P(q, L)$ measured in numerical simulations (see Methods):

$$P_{simpl}(q, L) = \big(P_0 + P_1 q^2\big)\, \mathbb{1}\big[|q| < q_{EA}^{(L)}\big] +$$
$$w^{(L)}\big(\delta(q - q_{EA}^{(L)}) + \delta(q + q_{EA}^{(L)})\big)/2\,, \quad (10)$$

where P_0 and P_1 are constants, $\mathbb{1}$ is the indicator function and $w^{(L)}$ is a weight enforcing normalization.[58]
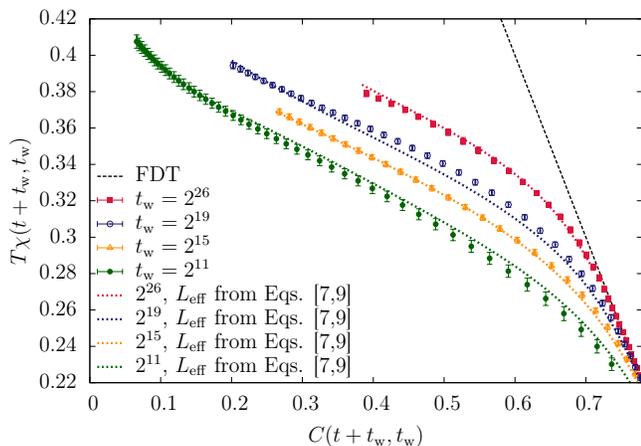
FIG. 4. As in Fig. 2 but L_{eff} is taken from the ansatz in (7) and (9), which improves on the single-time statics-dynamics dictionary based on $\xi(t_w)$ by considering a crossover to a $\xi(t+t_w)$-dominated regime.
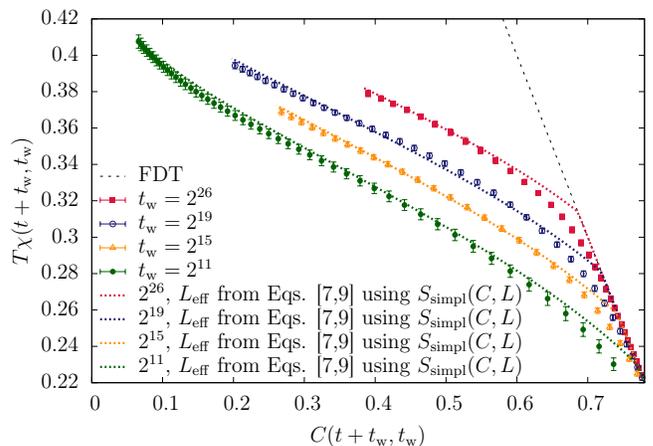

FIG. 5. As in Fig. 4 but this time we use the simplified $S_{\text{simpl}}(C, L)$ from (11). Note that dynamic data are well reproduced by (7) and (9), even in this simple approximation.

Integrating $P_{\text{simpl}}(q, L)$ twice we get

$$S_{\text{simpl}}(C, L) = \min \left[S_0(L) - P_0 C^2 - \frac{P_1}{6} C^4, 1 - C \right].$$
(11)

We take $S_0(L) = S(0, L)$ from the true $P(q, L)$. Recall that $S(0, L) = 1 - \overline{\langle |q| \rangle}_L$, see Appendix G. Instead, the L-independent P_0 and P_1 are fitted in order to obtain a $S_{\text{simpl}}(C, L)$ as similar as possible to the true $S(C, L)$: we get $P_0 = 0.167(1)$ and $P_1 = 0.46(3)$. In other words, $P_{\text{simpl}}(q)$ shares with the true distribution only four numeric features: normalization, first absolute moment $\overline{\langle |q| \rangle}_L$, $P_0 \simeq P(q = 0, L)$ which is essentially L-independent, and the second derivative $P_1 \simeq P''(q = 0, L)/2$. In particular, note that having $P_0 > 0$ is a crucial feature of the mean-field solution [59]. A direct measure for sizes $8 \leq L \leq 32$ returns the L-independent value $P(q = 0, L) = 0.167(5)$ [7] confirming the validity of our simplified description.

The outcome of this analysis is given in Fig. 5. It turns out that the simplified S_{simpl} in (11) is almost as effective as the true $S(C, L)$ in representing the non-equilibrium data through the effective size L_{eff} in (9). The only obvious disagreement is that (11) predicts a non-analytic behavior for the susceptibility χ at $C = q_{\text{EA}}^{(L_{\text{eff}})}$, which is not found in the non-equilibrium data. In other words, the effective size for times such that $C(t+t_w, t_w) \approx q_{\text{EA}}^{(L \approx 4\xi(t_w))}$ is large, but certainly L_{eff} is not infinite as demanded by (10).

Fortunately, even the crude description in (11) could lead to some interesting analysis. For instance, one could select pairs of times (t, t_w) such that $L_{\text{eff}}(t + t_w, t_w) = constant$. Then, $S(0, L_{\text{eff}})$ will be the same for all those points. Now, we note from (9) that $\xi(t + t_w)$ can vary by as much as a factor of two, for such points. It follows that $C(t + t_w, t_w)$ should vary significantly over this set

of times with fixed $L_{\text{eff}}(t + t_w, t_w)$. Hence, the crucial parameters P_0 and P_1 could be extracted. For instance, if the susceptibility $\chi(t + t_w, t_w)$ would turn out not to depend on $C(t + t_w, t_w)$ (while keeping L_{eff} fixed), this would mean $P_0, P_1 \approx 0$, in contrast with the mean field prediction $P_0 > 0$.

Discussion It was discovered some twenty years ago that experimental aging response functions carry information on Parisi's functional order parameter [11–13]. We now know that this connection between non-equilibrium and equilibrium physics relies on a very general mathematical property, stochastic stability [14, 15], shared by many glass models. However, experimental attempts to explore this connection encountered a major problem [17, 19]: an essentially uncontrolled extrapolation to infinite waiting time t_w is required.[60]

Here, we have proposed employing a statics-dynamics dictionary [5–8] to avoid uncontrolled extrapolations. Indeed, we have shown that the aging responses at finite t_w can be connected to the Parisi's order parameter as computed at equilibrium in a system of finite size.

We have shown that this GFDR-based SDD is essentially consistent with previous proposals [6–8] that focused on spatial correlation functions. This is an important consistency test. There is a caveat, though: when the probing time $t + t_w$ is such that one has $\xi(t + t_w) \gg \xi(t_w)$ for the coherence lengths, the GFDR-based SDD disagrees from previous dictionaries in that the size of the equivalent equilibrium system is $L_{\text{eff}} \sim \xi(t + t_w)$ (rather than $L_{\text{eff}} \sim \xi(t_w)$). In fact, we have found that the L_{eff} dependence on both length scales can be simply parameterized, recall (7) and (9).

At this point, the reader may wonder about the relationship between $L_{\text{eff}}(t + t_w, t_w)$ and the two-time correlation length $\zeta(t + t_w, t_w)$ obtained from the two-time/two-site correlation function introduced in Ref. [61, 62]. Indeed, we thoroughly studied the two-time/two-site corre-

lation function in [49] because it was a crucial ingredient for our previous SDD proposal [7, 8]. We found (see Fig. 12 in Ref. [49]) that $\zeta(t + t_\mathrm{w}, t_\mathrm{w})$ can grow, at most, as large as $\xi(t_\mathrm{w})$. Instead, the $L_\mathrm{eff}(t + t_\mathrm{w}, t_\mathrm{w})$ introduced here is asymptotically as large as $\xi(t + t_\mathrm{w})$.

On the other hand, the only previous SDD known to us that was based on (5) misses the $L_\mathrm{eff} \sim \xi(t + t_\mathrm{w})$ behavior [5]. There are a couple of possible reasons for this failure. For one, the time scales in Ref. [5] do not allow for length-scale separation $\xi(t + t_\mathrm{w}) \gg \xi(t_\mathrm{w})$. Besides, the SDD from Ref. [5] was obtained for two-dimensional spin glasses (which only have a paramagnetic phase). Therefore, the results of Ref. [5] are probably a manifestation of finite-time/finite-size scaling [53, 63].

Let us conclude by stressing that the three basic quantities analyzed in this work, namely the susceptibility $\chi(t + t_\mathrm{w}, t_\mathrm{w})$, the correlation function $C(t + t_\mathrm{w}, t_\mathrm{w})$ and the coherence length $\xi(t + t_\mathrm{w})$, have been obtained experimentally in a dynamic setting very similar to simulations (for χ and C, see Refs. [17, 19], for ξ see Refs. [42, 43]). We thus think that it should be possible to extract the spin-glass functional order parameter from already existing experimental data. Furthermore, GFDR have been studied as well in superspin glasses [10] and in a variety of soft condensed-matter systems [9, 28–36]. We therefore expect that our analysis will be of interest beyond the realm of spin glasses.

<center>**APPENDICES**</center>

<center>**Appendix A: Model and observables**</center>

We study the $D = 3$ Edwards-Anderson model, whose Hamiltonian is given by

$$\mathcal{H} = -\sum_{\langle \boldsymbol{x}, \boldsymbol{y} \rangle} J_{\boldsymbol{x}, \boldsymbol{y}} \sigma_{\boldsymbol{x}} \, \sigma_{\boldsymbol{y}} - H \sum_{\boldsymbol{x}} \sigma_{\boldsymbol{x}} \, . \quad \text{(A1)}$$

The spins $s_{\boldsymbol{x}} = \pm 1$ are placed on the nodes, $\boldsymbol{x}$, of a cubic lattice of linear size L and we set periodic boundary conditions. The couplings $J_{\boldsymbol{x}, \boldsymbol{y}} = \pm 1$, which join nearest neighbors only, are chosen randomly with 50% probability and are quenched variables. For each choice of the couplings (one "sample"), we simulate two independent copies of the system, $\{s_{\boldsymbol{x}}^{(1)}\}$ and $\{s_{\boldsymbol{x}}^{(2)}\}$. We denote by $\langle \cdots \rangle$ the average over the thermal noise and by $\overline{(\cdots)}$ the *subsequent* average over the samples. The model described by (A1) undergoes a SG transition at $H = 0$ and $T_{\text{c}} = 1.102(3)$ [64].

For our dynamical data we have run new non-equilibrium simulations on Memento, Janus and Janus II. We use heat-bath dynamics, in which one Monte Carlo step roughly corresponds to one picosecond of the experimental system [65]. See Appendix B for technical details of these simulations. The two main dynamical observables are the magnetization density $m_L(t + t_{\text{w}}) = \overline{\sum_{\boldsymbol{x}} \langle s_{\boldsymbol{x}}(t + t_{\text{w}}) \rangle}/V$ and the spin temporal correlation function $C_L(t + t_{\text{w}}, t_{\text{w}}; H) = \overline{\sum_{\boldsymbol{x}} \langle s_{\boldsymbol{x}}(t_{\text{w}}) s_{\boldsymbol{x}}(t + t_{\text{w}}) \rangle}/V$.

Equilibrium results at $T = 0.7$ are available for $L \leq 8 \leq 32$ [7]. In this case the main quantity is the proba-

bility density function $P(q, L)$ of the spin overlap q:

$$q \equiv \frac{1}{V} \sum_{\boldsymbol{x}} s_{\boldsymbol{x}}^{(1)} s_{\boldsymbol{x}}^{(2)} \, , \quad \overline{\langle q^k \rangle}_L = \int_{-1}^{1} \mathrm{d}q' \, (q')^k P(q', L) \, . \quad \text{(A2)}$$

In particular, we are interested in the integral

$$S(C, L) = \int_{C}^{1} \mathrm{d} \, C' \, x(C', L) \, , \; x(C, L) = \int_{0}^{C} \mathrm{d}q \, 2 P(q, L) \, . \quad \text{(A3)}$$

The $P(q, L)$ curves are easily described for finite L. They are symmetric under $q \leftrightarrow -q$, with two maxima at $\pm q_{\text{EA}}^{(L)}$ and a flat central region. In the thermodynamic limit, the two peaks turn into delta functions at $\pm q_{\text{EA}}^{(\infty)}$, which mark the maximum possible value of $|q|$. The size evolutions, as checked for $L \leq 32$ [7], are as follows: $q_{\text{EA}}^{(L)} - q_{\text{EA}}^{(\infty)} \propto L^{-\theta \approx 0.38}$ (at $T = 0.7$, $q_{\text{EA}}^{(\infty)} = 0.52(3)$ [8]), the width of the peaks at $\pm q_{\text{EA}}^{(L)}$ scales as $L^{-B \approx 0.28}$ while $P(q = 0, L)$ turns out to be greater than zero and L-independent.

<center>**Appendix B: Our simulations**</center>

Using heat-bath dynamics on the Janus, Janus II and Memento supercomputers, we consider the following numerical experiment. Starting from a completely random configuration of the spins at $T = 0.7$, we first let the system evolve in absence of a magnetic field, i.e. $H = 0$, for a waiting time t_{w}. As this t_{w} grows, the spins rearrange in amorphous magnetic domains of increasing average size ξ, as we show in Fig. 6 (ξ is computed with the ξ_{12} integral estimator described in Refs. [6, 49]). After this time t_{w}, we turn on a tiny field $H > 0$ and follow the response at a later time $t + t_{\text{w}}$.

We have considered five different values of t_{w}: $t_{\text{w}} = 2^{11}$ and $t_{\text{w}} = 2^{30}$ were simulated on Janus II; $t_{\text{w}} = 2^{26}, 2^{19}$ and 2^{15} on Janus (smaller systems were simulated on Memento, see below our study of size effects). Times are measured in units of Monte Carlo sweeps. The measuring times t were chosen as the integer part of $2^{i/4}$ for integer i (discarding repetitions). For each t_{w} we repeat the procedure described above for four values of the magnetic field: $H \in \{0, 0.02, 0.04, 0.08\}$ in the case of Memento and Janus I supercomputers and $H \in \{0, 0.01, 0.02, 0.04\}$ on Janus II. We considered exactly the same set of samples with each H and reused the same sequences of random numbers in an effort to eliminate sources of fluctuations.

Depending on the computer used, we simulated different system sizes, either $L = 80$ (on Memento and Janus I) or $L = 160$ (on Janus II). We simulated 647 samples for $L = 80$ (all t_{w} and H values). For $L = 160$, we used 55 samples for $t_{\text{w}} = 2^{11}$ and 335 samples for $t_{\text{w}} = 2^{30}$ [we also simulated 336 samples at $H = 0$ in order to compute $\xi(t_{\text{w}})$]. Notice that self-averaging means that one needs fewer samples for larger sizes. Previous works at
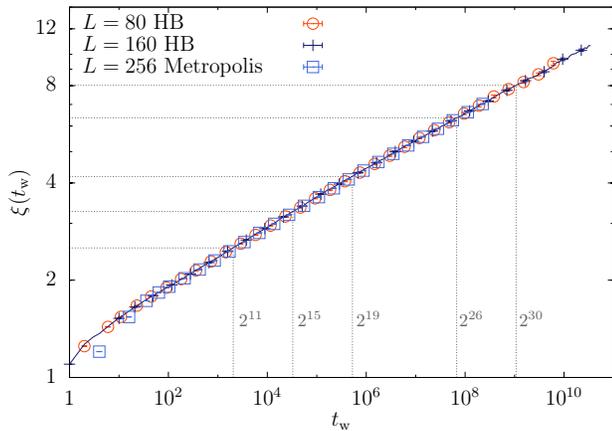
FIG. 6. Coherence length $\xi(t_{\mathrm{w}})$ versus waiting time t_{w} at $T = 0.7$ for different lattice sizes: $L = 80$ (data taken from [49]), $L = 160$ (new simulations) and $L = 256$ (Metropolis dynamics from [53], rescaling the x axis by a factor of 4 to compare with our heat-bath dynamics). The dashed lines aim to point out the different t_{w} (and their corresponding ξ) considered in this work.

$H = 0$ suggested that finite-size effects should be negligible, compared to our typical statistical accuracy, as long as we ensure that $L > 7\xi(t+t_{\mathrm{w}})$ [6]. As a new test of the validity of this statement, we compare our new results of $\xi(t_{\mathrm{w}})$ obtained with Janus II and $L = 160$ with previous works corresponding to $L = 80$ [49] and $L = 256$ [53] (see Fig. 6) finding no significant dependence on L in the studied range of t_{w}.

Appendix C: Computation of the linear susceptibility

The discussion on the GFDR requires the computation of the linear susceptibility, that is, of

$$\chi(t + t_{\mathrm{w}}, t_{\mathrm{w}}) = \left. \frac{\partial m(t + t_{\mathrm{w}})}{\partial H} \right|_{H=0}. \tag{C1}$$

With this aim, we measure $m(t, t_{\mathrm{w}})/H$ at several values of the external field, and use them to extract the $H \to 0$ limit. Indeed, since the Edwards-Anderson Hamiltonian is odd in the field around $H = 0$, one can write the magnetization in terms of odd powers of H, which allows us to separate the linear response χ from the non-linear responses

$$m(t + t_{\mathrm{w}}, t_{\mathrm{w}}; H) = H\chi(t+t_{\mathrm{w}}, t_{\mathrm{w}}) - \frac{H^3}{3!}\chi_{\mathrm{NL}}(t+t_{\mathrm{w}}, t_{\mathrm{w}}; H). \tag{C2}$$
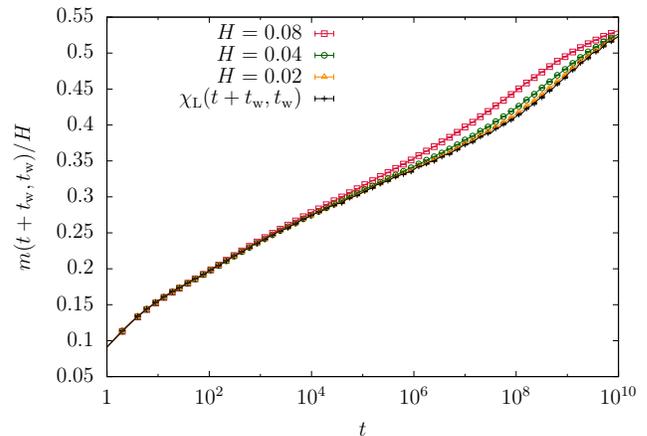
FIG. 7. Extraction of the linear susceptibility as a function of t from the $m(t+t_{\mathrm{w}}, t_{\mathrm{w}})/H$ data obtained at $H = 0.02$, 0.04 and 0.08. Data shown here corresponds to $t_{\mathrm{w}} = 2^{26}$. For the sake of visibility, only one every two measured times have been plotted in points.

In order to make some progress, we Taylor-expand $\chi_{\mathrm{NL}} = \chi_3 + \frac{H^2}{20}\chi_5 + \mathcal{O}(H^4)$, thus finding:

$$\begin{aligned} \frac{m(t + t_{\mathrm{w}}, t_{\mathrm{w}})}{H} =& \chi(t + t_{\mathrm{w}}, t_{\mathrm{w}}) - \frac{H^2}{3!}\chi_3(t + t_{\mathrm{w}}, t_{\mathrm{w}}) \\ & - \frac{H^4}{5!}\chi_5(t + t_{\mathrm{w}}, t_{\mathrm{w}}) + \mathcal{O}(H^6), \end{aligned} \tag{C3}$$

Therefore, if we measure m for three small fields and neglect higher-order contributions in H, we can extract $\chi(t + t_{\mathrm{w}}, t_{\mathrm{w}})$ from a set of three equations and three unknowns [by the same token, we obtain $\chi_3(t + t_{\mathrm{w}}, t_{\mathrm{w}})$ and $\chi_5(t + t_{\mathrm{w}}, t_{\mathrm{w}})$ as well, but these magnitudes will not be discussed herein]. We show in Fig. 7 $m(t+t_{\mathrm{w}}, t_{\mathrm{w}})/H$ and $\chi(t + t_{\mathrm{w}}, t_{\mathrm{w}})$ for one of our values of t_{w}.

Alternatively, instead of performing simulations at different H, one could have obtained $\chi(t + t_{\mathrm{w}}, t_{\mathrm{w}})$ directly from simulations at $H = 0$ using methods such as those described in Refs. [52, 66]. The drawback of this approach is that it would have required a much larger amount of samples in order to get equivalent statistical errors.

Appendix D: Smoothing and interpolating the data

The original data consisted of pairs $\{C(t+t_{\mathrm{w}}, t_{\mathrm{w}}), \chi(t+t_{\mathrm{w}}, t_{\mathrm{w}})\}$, where t takes some discrete values. However, if we reproduce Fig. 1 in the main text but using the raw measurements (see Fig. 8) we find much noisier curves. Indeed, data for successive times, although very correlated, displays random fluctuations. Besides, the statistical errors for $C(t+t_{\mathrm{w}}, t_{\mathrm{w}}; H = 0)$ and $C(t+t_{\mathrm{w}}, t_{\mathrm{w}}; H)$ are completely negligible compared to the errors in $Tm(t+t_{\mathrm{w}}, t_{\mathrm{w}}; H)/H$ (they are indistinguishable in the figure). We used these two facts to our benefit in
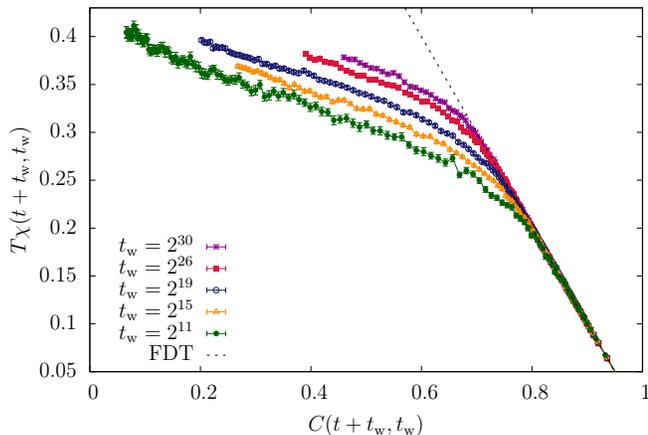
FIG. 8. Linear response $T\chi(t, t_w)$ versus $C(t + t_w, t_w)$ at $T = 0.7$ and five values of t_w using raw processed data (to be compared with Fig. 1 in the main text, which was obtained only after the smoothing of the simulation data at fixed H and an extrapolation to $H \to 0$).
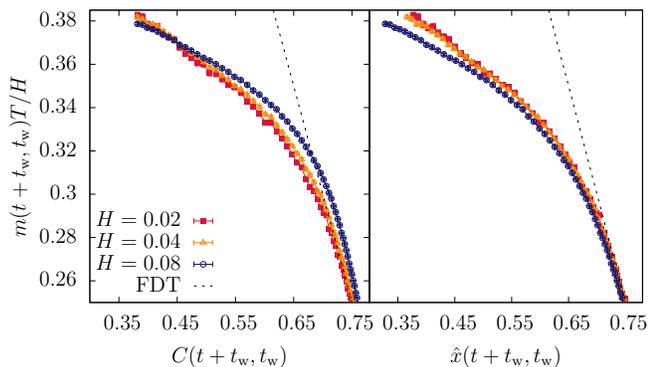

FIG. 9. Non-linear corrections in H to $T\chi(t + t_w, t_w)$ when plotted versus $C(t + t_w, t_w)$ (left) or $x(t + t_w, t_w) = C(t + t_w, t_w) + C(t + t_w, t_w; H)/2$ (right). Data corresponds to $t_w = 2^{26}$ and $T = 0.7$.

order to smooth and reduce the statistical errors of these curves. Let us describe our smoothing procedure step by step.

We fit our data for $Tm(t + t_w, t_w; H)/H$ to a smooth function of

$$\hat{x}(t + t_w, t_w) = \frac{C(t + t_w, t_w) + C(t + t_w, t_w; H)}{2} . \quad \text{(D1)}$$

This choice [instead of just $C(t + t_w, t_w)$], although irrelevant in the $H \to 0$ limit, turns out to reduce the non-linear corrections in H as we show in Fig. 9, and yields easier and more accurate fits.

Our chosen functional form is as follows. Let the quantity $Tm(t + t_w, t_w; H)/H$ be approximated by $f(\hat{x})$ (f depends on H and t_w, but we will write f nevertheless,

TABLE I. Information about the fits to Eqs. (D2,D3,D4).

t_w	H	N	N'	χ^2/DOF
	0.01	2	1	51.6822/127
2^{11}	0.02	2	1	43.9926/127
	0.04	2	1	45.6321/127
	0.02	2	1	33.1259/90
2^{15}	0.04	2	1	43.3823/90
	0.08	2	2	21.0832/89
	0.02	3	2	27.6364/115
2^{19}	0.04	3	2	25.8737/115
	0.08	3	3	31.6819/114
	0.02	2	1	29.5259/118
2^{26}	0.04	2	1	36.5544/118
	0.08	2	1	57.3693/118
	0.01	2	1	31.7369/126
2^{30}	0.02	3	3	24.7701/122
	0.04	3	2	33.0019/123

to keep the notation as light as possible):

$$f(\hat{x}) = f_L(\hat{x})\frac{1 + \tanh[Q(\hat{x})]}{2} + f_S(\hat{x})\frac{1 - \tanh[Q(\hat{x})]}{2} , \quad \text{(D2)}$$

with $Q(\hat{x}) = (\hat{x} - \hat{x}^*)/w$. In other words, there are two functional forms: f_S, adequate for small $\hat{x}$ and f_L, good for large $\hat{x}$. The crossover between the two functional forms takes place at $\hat{x}^* \approx 0.7$ in an interval of half-width $w \approx 0.04$ (although we keep $\hat{x}^*$ and w as fitting parameters). The functional form for small $\hat{x}$ are diagonal $[N, N]$ Padè approximants,

$$f_S(\hat{x}) = \frac{\sum_{k=0}^{N} b_k \hat{x}^k}{\sum_{k=0}^{N} a_k \hat{x}^k} . \quad \text{(D3)}$$

As for the region where deviations from the fluctuation-dissipation theorem are tiny, we chose a polynomial in $1 - \hat{x}$

$$f_L(\hat{x}) = (1 - \hat{x}) + \sum_{k=2}^{N'} c_k (1 - \hat{x})^k. \quad \text{(D4)}$$

We keep a_k, b_k, c_k as fitting variables.

Following Refs. [6, 49, 53, 63], we perform a fit considering only the diagonal part of the covariance matrix (we obtain χ^2/DOF significantly smaller than one, probably due to data correlation). Errors are computed following a jackknife procedure [we perform an independent fit for each jackknife block, and compute errors from the jackknife fluctuations of the fitted $f(\hat{x})$]. Our fits are reported in Table I.

Once each curve $Tm(t + t_w, t_w)/H$ is smoothed at each H, we extract the linear susceptibility following the procedure described in the previous Section. We show a comparison between the original and smoothed data in
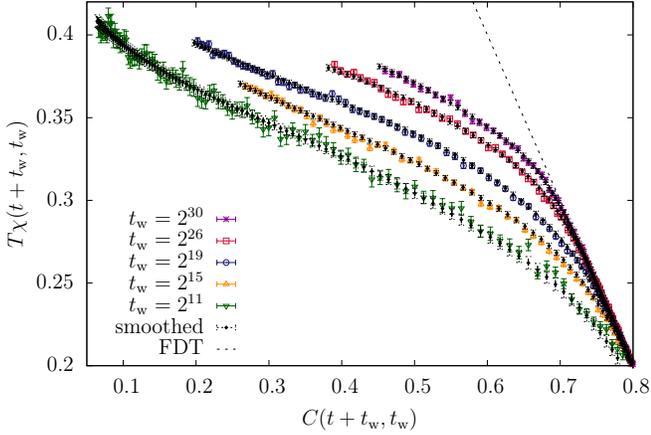
FIG. 10. Comparison between the original (in color and empty dots) and smoothed data (in black full dots) in the Linear response $T\chi(t + t_{\mathrm{w}}, t_{\mathrm{w}})$ versus $C(t + t_{\mathrm{w}}, t_{\mathrm{w}})$ curves. Data corresponds to $T = 0.7$ and five values of t_{w}.
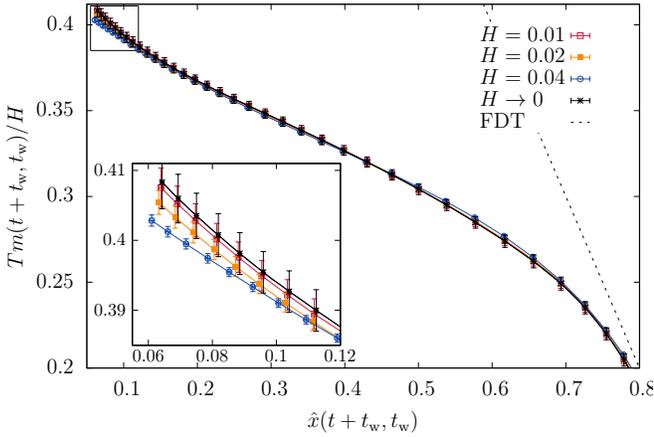
FIG. 11. $Tm(t + t_{\mathrm{w}}, t_{\mathrm{w}})/H$ versus $\hat{x}(t + t_{\mathrm{w}}, t_{\mathrm{w}})$ for several values of H (in color empty dots) and $t_{\mathrm{w}} = 2^{11}$, together with the extrapolation $H \to 0$ (in black crosses). The inset is a blow up of the region for large t/t_{w} in the square box.

Fig. 10. We found that in most the cases the extrapolated linear response $T\chi(t+t_{\mathrm{w}}, t_{\mathrm{w}})$ was compatible within the error with the smaller field considered. However, the extrapolation $H \to 0$ becomes particularly delicate and even changes the shape of the curve at large values of the t/t_{w} ratio, as we show in Fig. 11.

Appendix E: Fit of $S(C, L)$ and computation of L_{eff}

Part of our discussion in the main text seeks to find a relation between the linear response at finite t_{w} with the overlap distribution $P(q, L)$ in equilibrium at a finite size L_{eff}. That is,

$$T\chi(t + t_{\mathrm{w}}, t_{\mathrm{w}}) = S\big(C(t + t_{\mathrm{w}}, t_{\mathrm{w}}), L_{\mathrm{eff}}(t + t_{\mathrm{w}}, t_{\mathrm{w}})\big), \quad \text{(E1)}$$
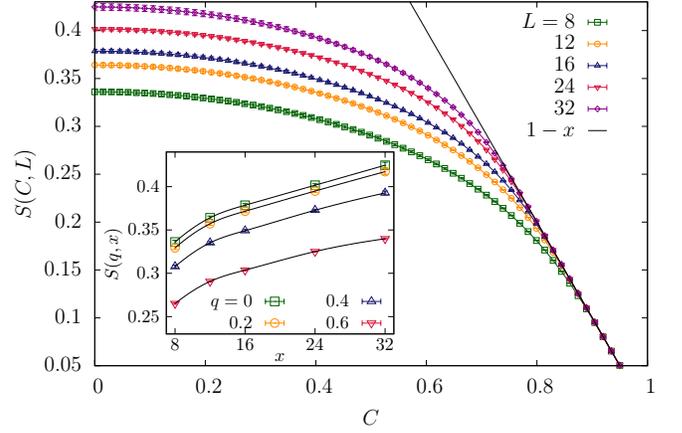

FIG. 12. $S(C, L)$ versus C for different system sizes obtained using (A3) and data from Ref. [7]. (Inset) Orthogonal cuts to the figure in the main panel plotted as function of L in color points together with the interpolating cubic spline curve along this variable.

where

$$S(C, L) = \int_C^1 dC' \, x(C', L), \ \ x(C, L) = \int_0^C dq \, 2P(q, L). \quad \text{(E2)}$$

We computed $S(C, L)$ by means of a numerical integration of the $P(q, L)$ discussed in Ref. [7] for $L = 8$, 12, 16, 24 and 32. We show $S(C, L)$ in the main panel of Fig. 12. In order to identify L_{eff} we needed a function $S(q, x)$ that is continuous both in C and in L, which we construct by computing a cubic spline[67] of the data along both variables (first in C and only then in L). Errors are computed using the jackknife method. We show some interpolation curves along the x variable in the inset of Fig. 12. Once $S(q, x)$ is at hand, $L_{\mathrm{eff}}(t + t_{\mathrm{w}}, t_{\mathrm{w}})$ can be extracted by looking for the x value that satisfies (E1) at each time t, fixing the off-equilibrium data $T\chi(t + t_{\mathrm{w}}, t_{\mathrm{w}})$ and $C(t, t_{\mathrm{w}})$.

Appendix F: Finite-size effects in the response

Up to now, finite-size effects have been investigated only for single-time correlation functions [and the related extraction of $\xi(t_{\mathrm{w}})$]. As far as we know, size effects were not studied previously in the response to a magnetic field $\chi(t + t_{\mathrm{w}}, t_{\mathrm{w}})$. In this context, it is somewhat worrying that we have identified a large length scale $L_{\mathrm{eff}} \approx 100$ (discussed below) in the regime where deviations from the FDT are incipient. For this reason, we have explicitly checked that our data does not suffer from finite-size effects in that region (as we show in Fig. 13) by comparing results from three system sizes, $L = 20$, 40 and 80, in the case of $t_{\mathrm{w}} = 2^{15}$, finding no finite-size dependence. For the smaller system sizes we considered 28000 samples for $L = 20$ and 12000 samples for $L = 40$.
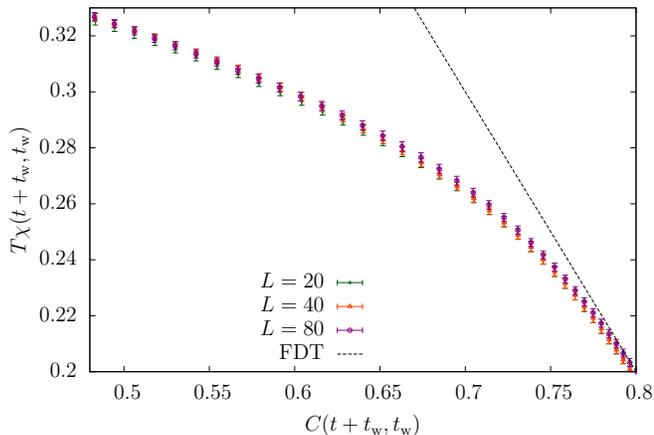
FIG. 13. Absence of finite-size effects in the response function $T\chi(t+t_{\mathrm{w}},t_{\mathrm{w}})$ versus $C(t+t_{\mathrm{w}},t_{\mathrm{w}})$ at $T=0.7$. Data from $L=20$, 40 and 80 are compared in the case of $t_{\mathrm{w}}=2^{15}$. All the points are compatible within the error bars.

Appendix G: A simple inequality

In the main text, we have used several times the inequality

$$S(C,L) \leq 1 - \overline{\langle |q| \rangle}_{L=\infty} \,. \qquad (G1)$$

Our purpose here is to remind the reader of its derivation, for the sake of completeness.

Let us first recall the notations used in the main text:

$$S(C,L) = \int_C^1 d\mathrm{C}'\, x(C',L)\,, \qquad (G2)$$

$$x(C,L) = \int_0^C \mathrm{d}q\, 2P(q,L)\,. \qquad (G3)$$

We start by noticing

$$S(C,L) \leq S(C=0,L)\,, \qquad (G4)$$

due to the inequality $x(C,L) \geq 0$ for the cumulative distribution. Next, we integrate by parts to find [recall that $P(q,L)=P(-q,L)$]

$$S(C=0,L) = 1 - \overline{\langle |q| \rangle}_L\,, \quad \overline{\langle |q| \rangle}_L \equiv \int_{-1}^1 \mathrm{d}q |q| P(q,L)\,. \qquad (G5)$$

Finally, to obtain the upper bound in (G1), we remark that $\overline{\langle |q| \rangle}_L$ is monotonically decreasing in L for a system with periodic boundary conditions.

Appendix H: The ferromagnetic case and conditions for validity of Eq. (5) of main text

Our SDD is based on Eq. (5) in the main text that we repeat here for readers convenience

$$T\chi(t+t_{\mathrm{w}},t_{\mathrm{w}}) = S\big(C(t+t_{\mathrm{w}},t_{\mathrm{w}}),L_{\mathrm{eff}}(t+t_{\mathrm{w}},t_{\mathrm{w}})\big)\,. \qquad (H1)$$
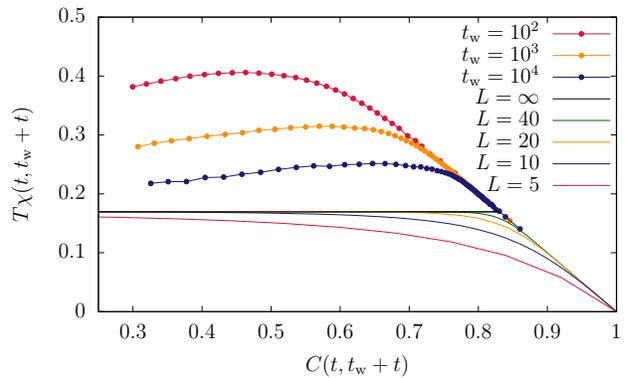
FIG. 14. Upper lines with points are data for $T\chi(t+t_{\mathrm{w}},t_{\mathrm{w}})$ versus $C(t+t_{\mathrm{w}},t_{\mathrm{w}})$ measured in the $D=2$ ferromagnetic Ising model at $T=2 \approx 0.88T_c$ (data from Ref. [52]). Lower lines are the equilibrium $S(C,L)$ for the same model and their thermodynamic limit $S(C,L=\infty)$. For this model Eq. (5) of main text can not be satisfied and the SDD does not exist.

Although for the $D=3$ Edwards-Anderson (EA) model the above equation can be satisfied for all our data, it is not obvious that this is the case for other models. In particular we show in Fig. 14 a simple case where (H1) can not be satisfied.

In Fig. 14 we show both equilibrium and non-equilibrium data for the $D=2$ ferromagnetic Ising model gathered at temperature $T=2 \approx 0.88T_c$. For the non-equilibrium data we reproduce correlation and responses already published in Ref. [52], while the equilibrium data have been obtained by running the Wolff algorithm [68]. The black line is the thermodynamical limit for the equilibrium data

$$S(C,\infty) = \min(1 - m(T)^2, 1 - C)$$

where $m(T)$ is the remanent magnetization.

It is clear from data in Fig. 14 that there is no L_{eff} size such that the non-equilibrium data can be matched with the equilibrium ones. This is a direct consequence of the fact that finite size effects in this model are such that $S(C,L) \leq S(C,\infty)$, while the dynamical curves show an excess of response, bringing them above $S(C,\infty)$.

In general the condition for the applicability of (H1) is that the dynamical curves must lie in the region of the $(T\chi,C)$ plane covered by the equilibrium functions $S(C,L)$. In the present case such a region is very narrow (as shown in Fig. 14 for $L \geq 5$) and the dynamical curves miss it. Luckily enough the analogous region for the $D=3$ EA model is very wide, and (H1) can be always satisfied on the timescales we have probed.

The very different behaviour between the above two models can be explained by noticing that there are at least two major sources of finite times effects:

- the first is the one discussed thoroughly in the main text. Its application to the ferromagnetic Ising model should give a really tiny effect, because the

$S(C, L)$ converges very fast to its thermodynamical limit;

- the second correction comes from the convergence of one-time quantities (e.g. the energy density) to their large time limit. This is the dominating one for the ferromagnetic Ising model, where the energy density decays as $E(t) - E(\infty) \propto \xi(t)^{-b}$, with $b = 1$. We expect this contribution to be much less important in the EA model, since the exponent is $b \simeq 2.6$ [49]. The ferromagnetic Ising model is very peculiar; in the general case, using the handwaiving argument that the exponent b equals the lower critical dimension, we expect $b > 1$ (e.g. $b = 2$ in models with continuous variables) and this correction to be much less relevant.

Appendix I: Extrapolating the effective size

We have shown in the main text that, for every $t_{\rm w}$ and small enough t, $L_{\rm eff}(t + t_{\rm w}, t_{\rm w})$ can be very large. This *short-time but large-size* effect arises when $C(t+t_{\rm w}, t_{\rm w}) \approx q_{\rm EA}^{L=4\xi(t_{\rm w})}$. In fact, for $t_{\rm w} = 2^{30}$ (our largest) we can compute $L_{\rm eff}$ without extrapolations only for the largest t.

The above observation begs the question: how large can $L_{\rm eff}$ be in this small-t regime? We provide here a crude extrapolation for our $t_{\rm w} = 2^{30}$ data, mostly based on the scaling laws found in [7].

We start by noticing that one could be tempted to extract the spin-overlap probability directly from the aging response. One can define the *dynamic overlap* probability density function:

$$P_{\rm dyn}(q; t_{\rm w}) = -\frac{1}{2} \left. \frac{\partial^2 T\chi(C, t_{\rm w})}{\partial C^2} \right|_{C=q} . \tag{I1}$$

Then, one could compare $P_{\rm dyn}$ with the equilibrium $P(q, L)$ at $q = C(t + t_{\rm w}, t_{\rm w})$. The weak point in this approach is that taking two derivatives of the curve $T\chi(C, t_{\rm w})$, which is subject to random errors, is very difficult.

Our way out will be to recall that the area under the peak of the $P(q, L)$ is approximately L-independent [7]. Therefore, we shall estimate the peak height (rather than the peak width).

Our efforts to locate the maximum (let alone the full curve) for $P_{\rm dyn}(q; t_{\rm w} = 2^{30})$ are documented in Fig. 15 (but the reader is warned to take the results *cum grano salis*). We note from Fig. 15 that the ratio of the height of the maxima for $t_{\rm w} = 2^{30}$ and $L = 32$ is $\sim 3.6/2.5$. Therefore, from the scaling of the peak width, $\propto L^{-B \approx 0.28}$, we extrapolate

$$L_{\rm eff} \sim 32 \times (3.6/2.5)^{\frac{1}{B}} \approx 118 , \tag{I2}$$

which is certainly larger than our maximum equilibrium size, $L = 32$.

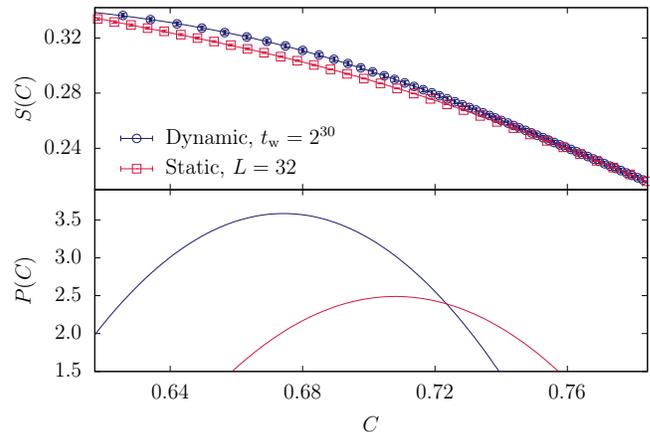FIG. 15. **Numerical attempt to locate the maximum of $P_{\rm dyn}(q, t_{\rm w} = 2^{30})$.** In the top panel, we compare the dynamic response $T\chi(C, t_{\rm w} = 2^{30})$ with the equilibrium curve $S(C, L = 32)$. The range of C covers the peak width of $P(q, L = 32)$ [7]. Since the curvature is clearly larger for $T\chi$ than for $S(C, L = 32)$, (I1) tells us that that the maximum of $P_{\rm dyn}(q; t_{\rm w} = 2^{30})$ is higher than the maximum of $P(q, L = 32)$. The lines correspond to diagonal fits to fourth order polynomials in C (we increased the order of the polynomial until the figure of merit diagonal-χ^2 for the fit of the dynamic response no longer decreased). The bottom panel shows the second derivative of the interpolating polynomials of the top panel, multiplied by $-1/2$. According to (I1), these derivatives should give us $P_{\rm dyn}(q, t_{\rm w})$ and $P(q, L)$. Indeed, the peak position and height in $P(q, L = 32)$ is very reasonably reproduced by this approach, see Ref. [7].

Appendix J: The simplified $S(C, L)$

In the main text, we wondered about the consequences of having at our disposal only a simplified approximation for $S(C, L)$:

$$S_{\rm simpl}(C, L) = \min \left[S_0(L) - P_0 C^2 - \frac{P_1}{6} C^4, 1 - C \right] . \tag{J1}$$

In the above equation, P_0 and P_1 are L-independent constants. All the depedence on the system size is in $S_0(L)$. In fact, $S_0(L)$ was obtained by fitting the actual data $S(C = 0, L = 8, 12, 16, 24, 32)$ to a quadratic polynomial in $L^{-\theta}$. We took $\theta = 0.38$ from Ref. [7] [recall that the maximum of the spin-overlap probability, $P(q, L)$ scales with L as $q_{\rm EA}^{(L)} - q_{\rm EA}^{(\infty)} \propto L^{-\theta}$]. Once $S_0(L)$ was known, we determined the constants P_0 and P_1 from a least-squares minimization of the difference between $S_{\rm simpl}(C, L)$ and the actual data.

[1] A. Cavagna, Physics Reports **476**, 51 (2009), arXiv:0903.4264.

[2] E. Vincent, J. Hammann, M. Ocio, J.-P. Bouchaud, and L. F. Cugliandolo, in *Complex Behavior of Glassy Systems*, Lecture Notes in Physics No. 492, edited by M. Rubí and C. Pérez-Vicente (Springer, 1997).

[3] G. F. Rodriguez, G. G. Kenning, and R. Orbach, Phys. Rev. Lett. **91**, 037203 (2003).

[4] V. Dupuis, F. Bert, J.-P. Bouchaud, J. Hammann, F. Ladieu, D. Parker, and E. Vincent, Pramana J. of Phys. **64**, 1109 (2005).

[5] A. Barrat and L. Berthier, Phys. Rev. Lett. **87**, 087204 (2001).

[6] F. Belletti, M. Cotallo, A. Cruz, L. A. Fernandez, A. Gordillo-Guerrero, M. Guidetti, A. Maiorano, F. Mantovani, E. Marinari, V. Martín-Mayor, A. M. Sudupe, D. Navarro, G. Parisi, S. Perez-Gaviro, J. J. Ruiz-Lorenzo, S. F. Schifano, D. Sciretti, A. Tarancon, R. Tripiccione, J. L. Velasco, and D. Yllanes (Janus Collaboration), Phys. Rev. Lett. **101**, 157201 (2008), arXiv:0804.1471.

[7] R. A. Baños, A. Cruz, L. A. Fernandez, J. M. Gil-Narvion, A. Gordillo-Guerrero, M. Guidetti, A. Maiorano, F. Mantovani, E. Marinari, V. Martín-Mayor, J. Monforte-Garcia, A. Muñoz Sudupe, D. Navarro, G. Parisi, S. Perez-Gaviro, J. J. Ruiz-Lorenzo, S. F. Schifano, B. Seoane, A. Tarancon, R. Tripiccione, and D. Yllanes (Janus Collaboration), J. Stat. Mech. **2010**, P06026 (2010), arXiv:1003.2569.

[8] R. A. Baños, A. Cruz, L. A. Fernandez, J. M. Gil-Narvion, A. Gordillo-Guerrero, M. Guidetti, A. Maiorano, F. Mantovani, E. Marinari, V. Martín-Mayor, J. Monforte-Garcia, A. Muñoz Sudupe, D. Navarro, G. Parisi, S. Perez-Gaviro, J. J. Ruiz-Lorenzo, S. F. Schifano, B. Seoane, A. Tarancon, R. Tripiccione, and D. Yllanes (Janus Collaboration), Phys. Rev. Lett. **105**, 177202 (2010), arXiv:1003.2943.

[9] H. Oukris and N. E. Israeloff, Nature Physics **06**, 135 (2010).

[10] K. Komatsu, D. L'Hôte, S. Nakamae, V. Mosser, M. Konczykowski, E. Dubois, V. Dupuis, and R. Perzynski, Phys. Rev. Lett. **106**, 150603 (2011), arXiv:1010.4012.

[11] L. F. Cugliandolo and J. Kurchan, Phys. Rev. Lett. **71**, 173 (1993).

[12] S. Franz and H. Rieger, Journal of Statistical Physics **79**, 749 (1995).

[13] E. Marinari, G. Parisi, F. Ricci-Tersenghi, and J. J. Ruiz-Lorenzo, Journal of Physics A: Mathematical and General **31**, 2611 (1998).

[14] S. Franz, M. Mézard, G. Parisi, and L. Peliti, Phys. Rev. Lett. **81**, 1758 (1998).

[15] S. Franz, M. Mézard, G. Parisi, and L. Peliti, Journal of Statistical Physics **97**, 459 (1999).

[16] E. Marinari, G. Parisi, F. Ricci-Tersenghi, and J. J. Ruiz-Lorenzo, J. Phys. A **33**, 2373 (2000).

[17] D. Hérisson and M. Ocio, Phys. Rev. Lett. **88**, 257202 (2002), arXiv:cond-mat/0112378.

[18] A. Cruz, L. A. Fernández, S. Jiménez, J. J. Ruiz-Lorenzo, and A. Tarancón, Phys. Rev. B **67**, 214425 (2003).

[19] D. Hérisson and M. Ocio, Eur. Phys. J. B **40**, 283 (2004), arXiv:cond-mat/0403112.

[20] G. Parisi, Phys. Rev. Lett. **43**, 1754 (1979).

[21] H. Kawamura, Phys. Rev. Lett. **90**, 237201 (2003).

[22] O. V. Billoni, S. A. Cannas, and F. A. Tamarit, Phys. Rev. B **72**, 104407 (2005).

[23] G. Parisi, Phys. Rev. Lett. **79**, 3660 (1997).

[24] J.-L. Barrat and W. Kob, EPL (Europhysics Letters) **46**, 637 (1999).

[25] J.-L. Barrat and L. Berthier, Phys. Rev. E **63**, 012503 (2000).

[26] L. Berthier, Phys. Rev. Lett. **98**, 220601 (2007).

[27] N. Gnan, C. Maggi, G. Parisi, and F. Sciortino, Phys. Rev. Lett. **110**, 035701 (2013).

[28] T. S. Grigera and N. E. Israeloff, Phys. Rev. Lett. **83**, 5038 (1999).

[29] L. Bellon, S. Ciliberto, and C. Laroche, EPL (Europhysics Letters) **53**, 511 (2001).

[30] C. Maggi, R. Di Leonardo, J. C. Dyre, and G. Ruocco, Phys. Rev. B **81**, 104201 (2010).

[31] C. Maggi, R. Di Leonardo, G. Ruocco, and J. C. Dyre, Phys. Rev. Lett. **109**, 097401 (2012).

[32] J. R. Gomez-Solano, A. Petrosyan, S. Ciliberto, R. Chetrite, and K. Gawędzki, Phys. Rev. Lett. **103**, 040601 (2009).

[33] P. Jop, J. R. Gomez-Solano, A. Petrosyan, and S. Ciliberto, Journal of Statistical Mechanics: Theory and Experiment **2009**, P04012 (2009).

[34] N. Greinert, T. Wood, and P. Bartlett, Phys. Rev. Lett. **97**, 265702 (2006).

[35] D. Bonn and W. K. Kegel, The Journal of Chemical Physics **118**, 2005 (2003).

[36] E. Dieterich, J. Camunas-Soler, M. Ribezzi-Crivellari, U. Seifert, and F. Ritort, Nat Phys **11**, 971 (2015).

[37] F. Belletti, M. Cotallo, A. Cruz, L. A. Fernandez, A. Gordillo, A. Maiorano, F. Mantovani, E. Marinari, V. Martín-Mayor, A. Muñoz Sudupe, D. Navarro, S. Perez-Gaviro, J. J. Ruiz-Lorenzo, S. F. Schifano, D. Sciretti, A. Tarancon, R. Tripiccione, and J. L. Velasco (Janus Collaboration), Comp. Phys. Comm. **178**, 208 (2008), arXiv:0704.3573.

[38] M. Baity-Jesi, R. A. Baños, A. Cruz, L. A. Fernandez, J. M. Gil-Narvion, A. Gordillo-Guerrero, D. Iniguez, A. Maiorano, F. Mantovani, E. Marinari, V. Martín-Mayor, J. Monforte-Garcia, A. Muñoz Sudupe, D. Navarro, G. Parisi, S. Perez-Gaviro, M. Pivanti, F. Ricci-Tersenghi, J. J. Ruiz-Lorenzo, S. F. Schifano, B. Seoane, A. Tarancon, R. Tripiccione, and D. Yllanes (Janus Collaboration), Comp. Phys. Comm **185**, 550 (2014), arXiv:1310.1032.

[39] K. Gunnarsson, P. Svedlindh, P. Nordblad, L. Lundgren, H. Aruga, and A. Ito, Phys. Rev. B **43**, 8199 (1991).

[40] M. Palassini and S. Caracciolo, Phys. Rev. Lett. **82**, 5128 (1999), arXiv:cond-mat/9904246.

[41] H. G. Ballesteros, A. Cruz, L. A. Fernandez, V. Martín-Mayor, J. Pech, J. J. Ruiz-Lorenzo, A. Tarancon, P. Tellez, C. L. Ullod, and C. Ungil, Phys. Rev. B **62**, 14237 (2000), arXiv:cond-mat/0006211.

[42] Y. G. Joh, R. Orbach, G. G. Wood, J. Hammann, and E. Vincent, Phys. Rev. Lett. **82**, 438 (1999).

[43] F. Bert, V. Dupuis, E. Vincent, J. Hammann, and J.-P. Bouchaud, Phys. Rev. Lett. **92**, 167203 (2004).

[44] L. Berthier, G. Biroli, J.-P. Bouchaud, L. Cipelletti, D. El Masri, D. L'Hôte, F. Ladieu, and M. Pierno, Science **310**, 1797 (2005).

[45] A. P. Young, *Spin Glasses and Random Fields* (World Scientific, Singapore, 1998).

[46] A. Cruz, J. Pech, A. Tarancon, P. Tellez, C. L. Ullod, and C. Ungil, Comp. Phys. Comm **133**, 165 (2001), arXiv:cond-mat/0004080.

[47] A. T. Ogielski, Phys. Rev. B **32**, 7384 (1985).

[48] F. Belletti, M. Guidetti, A. Maiorano, F. Mantovani, S. F. Schifano, R. Tripiccione, M. Cotallo, S. Perez-Gaviro, D. Sciretti, J. L. Velasco, A. Cruz, D. Navarro, A. Tarancon, L. A. Fernandez, V. Martín-Mayor, A. Muñoz-Sudupe, D. Yllanes, A. Gordillo-Guerrero, J. J. Ruiz-Lorenzo, E. Marinari, G. Parisi, M. Rossi, and G. Zanier (Janus Collaboration), Computing in Science and Engineering **11**, 48 (2009).

[49] F. Belletti, A. Cruz, L. A. Fernandez, A. Gordillo-Guerrero, M. Guidetti, A. Maiorano, F. Mantovani, E. Marinari, V. Martín-Mayor, J. Monforte, A. Muñoz Sudupe, D. Navarro, G. Parisi, S. Perez-Gaviro, J. J. Ruiz-Lorenzo, S. F. Schifano, D. Sciretti, A. Tarancon, R. Tripiccione, and D. Yllanes (Janus Collaboration), J. Stat. Phys. **135**, 1121 (2009), arXiv:0811.2864.

[50] In fact, the correlation functions decay exponentially with distance. Therefore, with periodic boundary conditions, size effects should decay exponentially with L/ξ. Indeed, an explicit computation shows that, to our accuracy level, size corrections are completely negligible when $L > 7\xi$ [6].

[51] G. Parisi, F. Ricci-Tersenghi, and J. J. Ruiz-Lorenzo, Eur. Phys. J. **11**, 317 (1999), arXiv:cond-mat/9811374.

[52] F. Ricci-Tersenghi, Phys. Rev. E **68**, 065104 (2003).

[53] L. A. Fernández and V. Martín-Mayor, Phys. Rev. B **91**, 174202 (2015).

[54] M. Manssen, A. K. Hartmann, and A. P. Young, Phys. Rev. B **91**, 104430 (2015), arXiv:1501.06760.

[55] M. Wittmann and A. P. Young, Journal of Statistical Mechanics: Theory and Experiment **2016**, 013301 (2016).

[56] M. Mézard, G. Parisi, and M. Virasoro, *Spin-Glass Theory and Beyond* (World Scientific, Singapore, 1987).

[57] The reader will note that data for $t_{\mathrm{w}} = 2^{19}$ are slightly off, in Fig. 3. We attribute the effect to a strong statistical fluctuation, enhanced by the fact that all data points with the same t_{w} are extremely correlated.

[58] Note that the delta peak in (10) is a reasonable expectation only for an infinite system (see Methods).

[59] E. Marinari, G. Parisi, F. Ricci-Tersenghi, J. J. Ruiz-Lorenzo, and F. Zuliani, J. Stat. Phys. **98**, 973 (2000), arXiv:cond-mat/9906076.

[60] See Ref. [69] for an experimental attempt to measure Parisi's functional order parameter, unrelated to GFDR.

[61] L. C. Jaubert, C. Chamon, L. F. Cugliandolo, and M. Picco, J. Stat. Mech. **2007**, P05001 (2007).

[62] C. Chamon and L. F. Cugliandolo, J. Stat. Mech. **2007**, P07022 (2007).

[63] M. Lulli, G. Parisi, and A. Pelissetto, Phys. Rev. E **93**, 032126 (2016).

[64] M. Baity-Jesi, R. A. Baños, A. Cruz, L. A. Fernandez, J. M. Gil-Narvion, A. Gordillo-Guerrero, D. Iniguez, A. Maiorano, F. Mantovani, E. Marinari, V. Martín-Mayor, J. Monforte-Garcia, A. Muñoz Sudupe, D. Navarro, G. Parisi, S. Perez-Gaviro, M. Pivanti, F. Ricci-Tersenghi, J. J. Ruiz-Lorenzo, S. F. Schifano, B. Seoane, A. Tarancon, R. Tripiccione, and D. Yllanes (Janus Collaboration), Phys. Rev. B **88**, 224416 (2013), arXiv:1310.2910.

[65] J. A. Mydosh, *Spin Glasses: an Experimental Introduction* (Taylor and Francis, London, 1993).

[66] C. Chatelain, Journal of Physics A: Mathematical and General **36**, 10739 (2003).

[67] We do not used the so-called "natural" cubic spline. Instead, we fixed the first and last derivative of the interpolating function from three points of a parabolic fit.

[68] U. Wolff, Phys. Rev. Lett. **62**, 361 (1989).

[69] Y. G. Joh, R. Orbach, and J. Hammann, Phys. Rev. Lett. **77**, 4648 (1996).